Heliyon 9 (2023) e15237

Contents lists available at ScienceDirect

Heliyon

journal homepage: www.cell.com/heliyon

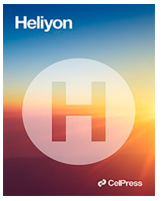

Research article

Sequential multi-parametric MRI in assessment of the histological subtype and features in the malignant pleural mesothelioma xenografts

Zhenghua Zhang [a], Shasha Shen [a], Jiyao Ma [a], Tianfu Qi [a], Chao Gao [a], Xiong Hu [b], Dan Han [a,*], Yilong Huang [a]

[a] Medical Imaging Department, First Affiliated Hospital of Kunming Medical University, Kunming, 650000, China
[b] Pathology Department, First Affiliated Hospital of Kunming Medical University, Kunming, 650000, China

ARTICLE INFO

Keywords:
Multiparametric MRI
Malignant pleural mesothelioma
Histological subtype
Microvessel density
Necrosis

ABSTRACT

Objective: It is still a challenge to find a noninvasive technique to distinguish the histological subtypes of malignant pleural mesothelioma (MPM) and characterize the development of related histological features. We investigated the potential value of multiparametric MRI in the assessment of the histological subtype and development of histologic features in the MPM xenograft model.

Methods: MPM xenograft models were developed by injecting tumour cells into the right axillary space of nude mice. The T1, T2, R2*, T2*, apparent diffusion coefficient (ADC), true diffusion coefficient (D), pseudo diffusion coefficient (D*), and perfusion fraction (f) at 14 d, 28 d, and 42 d were measured and compared between the epithelial and biphasic MPM. Correlations between multiparametric MRI parameters and histologic features, including necrotic fraction (NF) and microvessel density (MVD), were analysed.

Results: This study found that T2, T2* and IVIM-DWI parameters can reflect the spatial and temporal heterogeneity of MPM. Compared to the epithelial MPM, T2 and T2* were higher and ADC, D, D*, and f were lower in the biphasic MPM ($P < 0.05$). MRI parameters were different in different stages of epithelial and biphasic MPM. Moderate correlations were found between ADC and tumor volume and NF in the epithelial MPM, and there was a correlation between f and tumor volume and NF and MVD in the two groups.

Conclusion: MRI parameters changed with tumor progression in a xenograft model of MPM. MRI parameters may provide useful biomarkers for evaluating the histological subtype and histological features development of MPM.

1. Introduction

Malignant pleural mesothelioma (MPM) is an aggressive and lethal cancer related to asbestos exposure [1,2]. MPM has a poor prognosis, with survival rates ranging from 4 to 17 months from diagnosis [3]. The most common histological subtypes of MPM are epithelioid, biphasic, and sarcomatoid [4]. The histological subtype is among the most important prognostic factors in MPM, and the

* Corresponding author.
E-mail address: kmhandan@sina.com (D. Han).

https://doi.org/10.1016/j.heliyon.2023.e15237
Received 27 October 2022; Received in revised form 5 February 2023; Accepted 30 March 2023
Available online 11 April 2023

epithelioid subtype has a better prognosis than another subtype [5]. A previous study showed that tumor necrosis and vascularization are also important prognostic factors for MPM survival [6]. It is still a challenge to find a noninvasive technique to distinguish the histological subtypes of MPM and characterize the development of related histological features.

Medical imaging plays an important role in the diagnosis, staging, and follow-up of MPM [7]. Computed tomography (CT) is widely used as one of the leading imaging modalities in the chest examination of MPM. However, the similarities in morphology and enhancement features between MPM and benign lesions, such as pleural thickening and pleural cavity effusion, limit the effectiveness of CT [8]. MRI has been proven to be useful in the diagnosis of tumors. T1 mapping and T2 mapping can be used to quantitatively distinguish benign and malignant tumors and evaluate the efficacy [9,10]. Since the relaxation behavior of water is changed by the change in the amount of deoxyhemoglobin in the blood, the state of the iron ion in the heme subunit changes from the diamagnetism low spin state at high PO_2 to paramagnetism. The relaxation rate [R2*] of blood oxygen level-dependent (BOLD) sensitively evaluates the concentration of deoxyhemoglobin in the tissue, so R2* can be used to reflect the level of hypoxia in tumor tissues [11,12]. Intravoxel incoherent motion (IVIM), a new diffusion-weighted imaging (DWI) model, is used to calculate quantitative parameters representing water molecule diffusion and microcirculation perfusion information of tumors using a biexponential model. As a noninvasive examination, IVIM-DWI takes into account both the diffusion motion of water molecules and the perfusion effect of blood in microcirculation capillaries, which can more accurately and truly display the diffusion motion of water molecules and quantify this process. Compared with the ordinary single index model, ivim-DWI can better fit the attenuation of image signals on DWI and reveal tissue heterogeneity. This reflects the microscopic changes in histopathophysiology [13]. Studies have shown that IVIM-DWI parameters may replace dynamic contrast-enhanced magnetic resonance imaging (MRI) to detect the tissue perfusion rate [14,15]. Based on these promising studies, we hypothesize that multiparameter MRI can quantitatively evaluate the histological subtypes of MPM and its related histological feature development.

In this study, we used T1 mapping, T2 mapping, BOLD, and IVIM-DWI to distinguish MPM histological subtypes and evaluate histological feature development. In addition, we compared the MRI parameters with the tumor necrotic fraction (NF) and microvessel density (MVD) of MPM xenografts.

2. Methods

2.1. Cell culture

Human epithelioid MPM cells, NCI-H226, and human biphasic MPM cells, MSTO-211H, were obtained from American Type Culture Collection (Rockville, MD, United States). RPMI-1640 medium (Gibco, Grand Island, NY) was used for H226 and MSTO-211H cells. The culture media used for the experiments were supplemented with 10% heat-inactivated fetal bovine serum and 1% penicillin–streptomycin (Invitrogen, Carlsbad, CA). Cells were cultivated in the medium at 37 °C in a humidified environment of 5% CO_2.

2.2. Animal model

All of the animal experiments were approved by the Institutional Animal Care and Use Committee. The mice were raised under

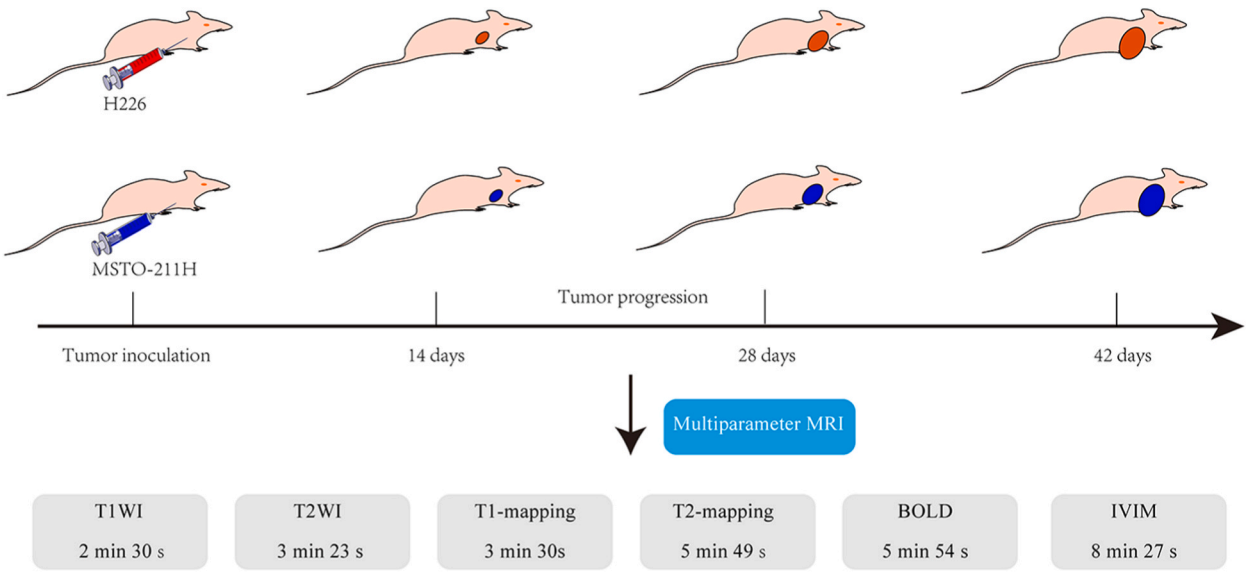

Fig. 1. Schedule of multiparameter MRI acquisition and tumor progression in H226 and MSTO-211H mice. H226 or MSTO-211H cells were implanted in the axilla of nude mice. At 14, 28, and 42 days after tumor inoculation, nude mice were scanned with multiparameter MRI.

specific pathogen-free conditions and kept at ambient temperature (24–26 °C) and humidity (30–50%) constant. Sterilized food and water were provided to all nude mice. We randomly divided forty-two female BALB/c-nu/nu mice (4–6 weeks old) into two groups, the H226 group (n = 21) and the MSTO-211H group (n = 21). The MPM xenografts were developed by injecting approximately 5×10^6 cells into the right axillary space of the nude mice. Multiparameter magnetic resonance examination was performed at 14 days (n = 7), 28 days (n = 7), and 42 days (n = 7) after tumor inoculation (Fig. 1). All mice were euthanized after MRI examination, and the tumor tissue was excised and prepared for histological evaluation. The long diameter (a) and short diameter (b) of the tumor are measured in the anatomical image. Tumor volume was calculated as $a \times b^2 \times 0.52$ [16].

2.3. MR data acquisition

MRI experiments were performed on a 3.0 T MR scanner (Achieva 3.0T Tx, Philips Healthcare, Best, Netherlands) using a dedicated mouse coil with an inner diameter of 50 mm (CG-MUC43-H300-AP, Chenguang Medical Technologies Co., LTD, Shanghai, China). After anaesthetization by an intraperitoneal injection of pentobarbital sodium (45 mg/kg), the mice were placed in a standard prone position, and subcutaneous xenograft tumors clicked to the platform of the coil to mitigate the possibility of motion artifacts. Warm water and cotton were used to maintain the mouse's body temperature. Multiparameter MRI included T1-weighted imaging (T1WI), T2-weighted imaging (T2WI), T1-mapping, T2-mapping, BOLD, and IVIM-DWI. The parameters of these MRI protocols are summarized in Table 1. During the MRI scan, we used fixed mouse positions and angles and the same thickness and spacing to ensure tumour position and angle was similar each time. If the movement artefact still occurred, mice were re-scanned with MRI 3 h after waking.

2.4. Image analyses

All raw MR images were processed on a commercially available workstation (Advantage Windows 4.6, GE Medical Systems, USA). T1WI and T2WI are used to observe the shape, size and location of the tumor. Through postprocessing software, the original T1 mapping and T2 mapping data were generated into T1 and T2 maps, and then the T1 and T2 values of the corresponding tumor region of interests (ROI) were obtained from T1 and T2 maps directly. The R2* and T2* values of the tumor tissue can be obtained in the BOLD. In addition to IVIM-DWI parameters, the apparent diffusion coefficient (ADC), true diffusion coefficient (D), pseudo diffusion coefficient (D*), and perfusion fraction (f) were calculated using the biexponential mode. All MRI parameters of the whole tumor were obtained on ROI. The ROIs of all images were drawn manually and blindly at the same level and position by two radiologists with over 5 years of experience in MRI diagnostics. Considering the tumor heterogeneity of MPM, the ROI of this study was selected as the three solid component regions of the largest tumor layer. The average of the three measurements of each ROI was used for analysis.

Table 1
MRI scan parameters.

Images	Axial T1WI	Axial T2WI	Coronal T2WI	T1mapping	T2mapping	BOLD	DWI-IVIM
Pulse sequence	SE	TSE	TSE	TSE	TSF	FFE	SE-EPI
TR (ms)	579	2288	1466	5000	1249 ms	735	710
TE (ms)	15	103	62	20	9、18、27、36、45、54、63、72 ms	2.5 ms, 4.6 ms, 6.7 ms, 8.8 ms, 10.9 ms, 13.0 ms, 15.1 ms, 17.2 ms, 19.3 ms, 21.4 ms, 23.5 ms, 25.6 ms	63
TI (ms)	/	/	/	250、500、750、1000、2000、3000	/	/	/
ST (mm)	2	2	2	2	2	2	2
SL (mm)	1	1	1	1	1	1	1
b-value (s/mm)	/	/	/	/	/	/	0, 10, 20, 30, 50, 100, 200, 400, 600, 800, 1000, 1200
Matrix	256 × 320	320 × 320	256 × 256	143 × 112	256 × 205	256 × 205	72 × 55
Voxel	0.156	0.125	0.156	0.35	0.195	0.195	0.69
FOV (mm2)	50 × 40	40 × 40	40 × 40	50 × 39	50 × 40	50 × 40	50 × 38
Flip angle	90°	90°	90°	180°	90°	30°	90°
Number of signal averaged	4	6	5	1	1	6	6

T1WI, T1-weighted imaging; T2WI, T2-weighted imaging; BOLD, blood oxygen level dependent; IVIM-DWI, Intravoxel incoherent motion-diffusion weighted imaging; TR, time of repetition; TE, echo time; TI, inversion time; ST, slice thickness; SL, slice increment; FOV, field of view.

2.5. Histopathological analysis

Animals in the H226 group and MSTO-211H group were sacrificed after image acquisition. The entire tumor was excised and fixed in 10% formalin for 48 h. The fixed tumor tissue was embedded in paraffin and cut into 5 μm sections. CD34 staining was performed on areas containing viable tumor tissues. Microvessel endothelial cells were identified by using CD34 staining. Three regions with the densest anti-CD34-positive blood vessels were found, and then the total MVD of the tumor was counted by magnifying 20 times [17]. In addition, hematoxylin and eosin (HE) staining was used to delineate the tumor pathological subtype and necrosis. The necrotic fraction was the average of the ratio of the tumor necrosis area to the total area in the three sections [18]. ImageJ (version 1.53a, USA) was used to analyse pathological images to detect NF and MVD.

2.6. Statistical analysis

SPSS version 22.0 was used to perform the analysis. The intraclass correlation coefficient (ICC) was used to evaluate the consistency of interobserver. The Mann−Whitney *U* test was used to compare differences in the T1, T2, R2*, T2*, ADC, D, D*, f, volume, NF and MVD of tumors between the H226 group and the MSTO-211H group. Spearman's rank correlations were computed between histological features and different MR parameters. A p value < 0.05 was reported to be statistically significant.

3. Result

3.1. Comparison of MRI parameters between the H226 and MSTO-211H groups

The ICC of the interobserver was 0.910 (95% CI (0.864–0.941), $P < 0.001$), and repeatability was excellent. The T1, T2, R2*, T2 values and IVIM-DWI parameters of the H226 and MSTO-211H groups are summarized in Table 2. T2 and T2* in the MSTO-211H group were higher than those in the H226 group, and the difference was statistically significant (all $P < 0.05$). Among the IVIM-DWI parameters, the ADC, D, D* and f values of the MSTO-211H group were lower than those of the H226 group (all $P < 0.05$). However, the difference in T1 and R2* values between the two groups was not statistically significant (all $P > 0.05$).

3.2. Sequential measurements of MRI parameters in the H226 and MSTO-211H groups

The results of sequential measurements of T1, T2, R2*, T2 values and IVIM-DWI parameters of both the H226 and MSTO-211H groups at three time points are summarized in Figs. 2 and 3. No significant differences were found in T1, T2, R2* and T2* at any follow-up time points in the H226 and MSTO-211H groups. Both ADC and D decreased significantly at 28 and 42 days compared with the values at 14 days (all $P < 0.05$) in the H226 group. In the MSTO-211H group, there were no significant differences among all different timepoints in the MRI parameters (all $P > 0.05$). Compared with that at 14 days, the D* at 28 days and 42 days increased significantly in the H226 and MSTO-211H groups, and the f value markedly increased at 28 and 42 days compared with that at 7 days (all $P < 0.05$). However, in the MSTO-211H group, f showed a significant decrease at 28 and 42 days (all $P > 0.05$).

3.3. Comparison of the development of tumor volume, NF, and MVD between the H226 and MSTO-211H groups

The tumor volume, NF and MVD in the H226 group were significantly smaller than those in the MSTO-211 group at the total and each time point (Fig. 4, all $P < 0.05$). Compared with 14 days, the NF and MVD of the H226 group were slightly increased at 28 days ($P = 0.124$) and significantly increased at 42 days ($P = 0.007$). The NF and MVD of the MSTO-211H group increased significantly at 28 and 42 days ($P = 0.018$ and 0.000).

3.4. Correlation of tumor volume, NF and MVD with MRI parameters

Tumor volume, NF and MVD showed a significant negative correlation with ADC and D but a positive correlation with f in the H226 group. Both ADC and D showed a good relationship with NF (Table 3). A moderate relationship was observed between ADC and tumor volume ($r = -0.53$, $P = 0.000$) and NF ($r = -0.508$, $P = 0.000$). However, no correlation was observed between the T1, T2, R2*, and

Table 2
Comparisons of MRI parameters of nude mice with xenograft MPM between different histological subtypes.

Histological subtype	T1 (ms)	T2 (ms)	R2* (Hz)	T2* (ms)	ADC ($\times 10^{-3}$ mm^2/s)	D ($\times 10^{-3}$ mm^2/s)	D*($\times 10^{-3}$ mm^2/s)	f (%)
H226 (n = 21)	1281.13 ± 59.21	86.69 ± 7.15	94.35 ± 7.84	11.67 ± 1.34	0.93 ± 0.14	0.81 ± 0.19	215.44 ± 61.87	25.28 ± 4.56
MSTO-211H (n = 21)	1222.46 ± 54.86	92.73 ± 6.61	91.81 ± 9.52	15.10 ± 1.74	0.81 ± 0.12	0.70 ± 0.15	158.66 ± 54.99	19.44 ± 4.02
p	0.224	0.045	0.199	0.02	0.003	0.007	0.029	0.016

Note: n, numbers of tumors. All values were expressed as mean ± standard deviation.

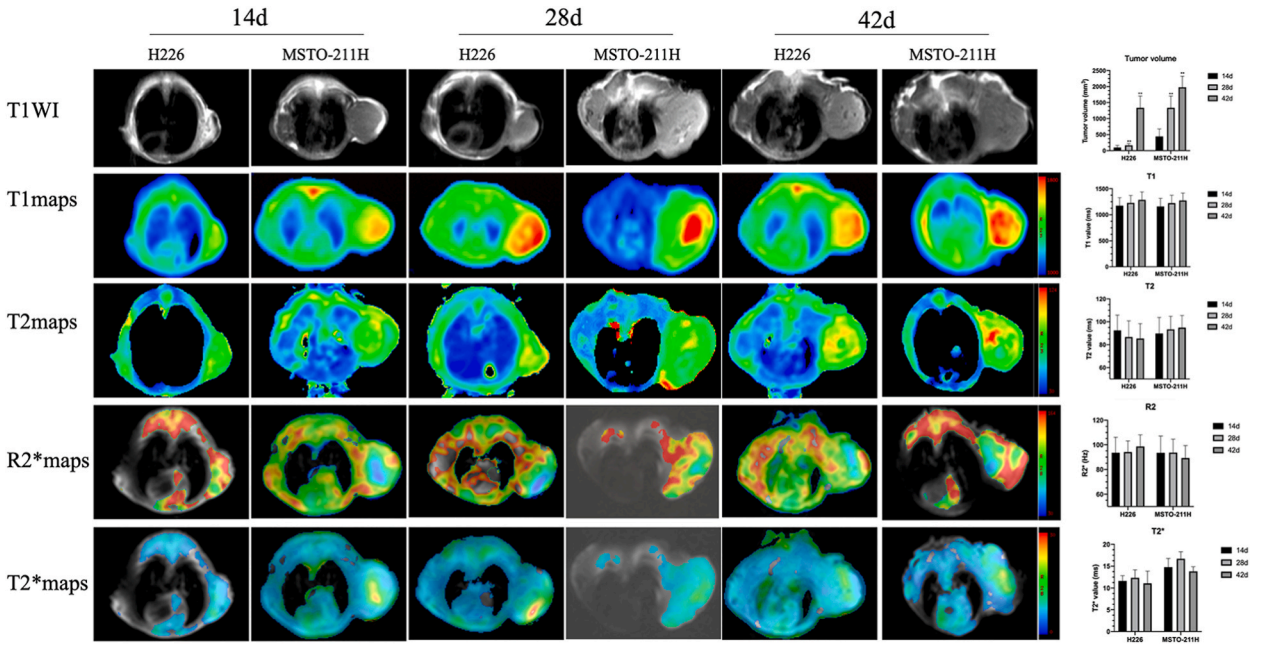

Fig. 2. T1WI (first row), T1(second row), T2 (third row), R2* (fourth row) and T2* (fifth row) maps of two MPM histological subtypes at 14 days, 28 days and 42 days. Data are reported as the mean ± standard deviation of the mean. *$P < 0.05$ compared with 14 days, **$P < 0.01$ compared with 14 days (Mann–Whitney *U* test).

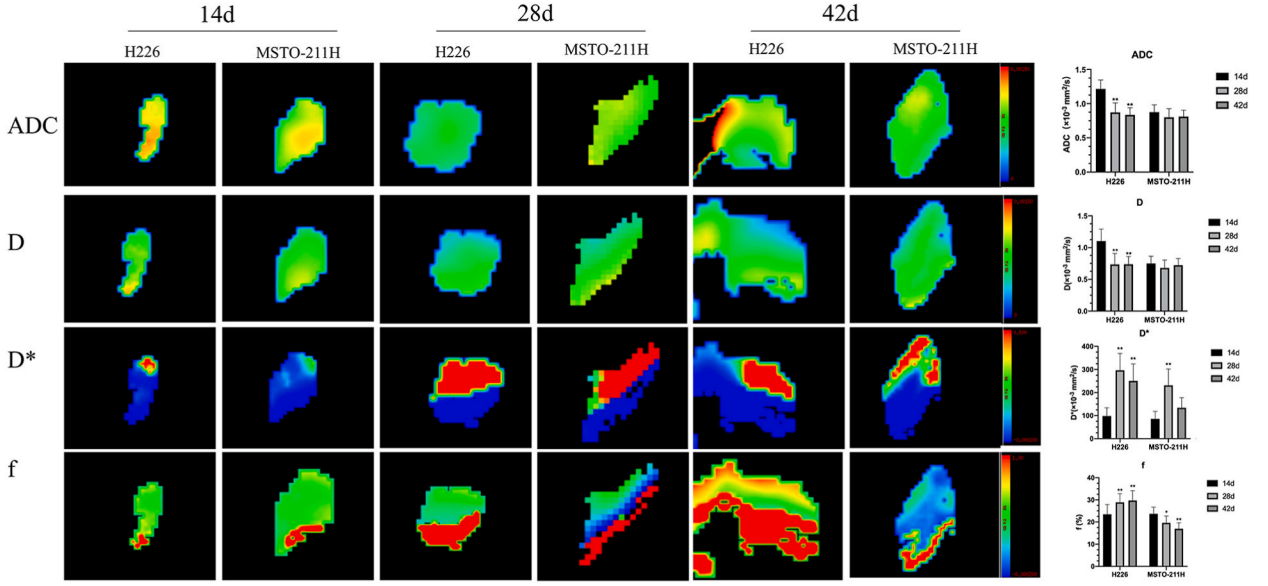

Fig. 3. IVIM-DWI parameter maps of two MPM histological subtypes at 14 days, 28 days and 42 days. ADC, first row; D, second row; D*, third row; f, fourth row. Data are reported as the mean ± standard deviation of the mean. *$P < 0.05$ compared with 14 days, **$P < 0.01$ compared with 14 days (Mann–Whitney *U* test).

T2* values and NF. There was also no correlation between T1, T2, R2*, T2* value parameters and histological MVD.

Only f had a negative correlation with tumor volume, NF and MVD in the MSTO-211H group, with a moderate relationship (r = −0.560, P = 0.009; r = −507, P = 0.001; r = −0.554, P = 0.000, respectively) (Table 3). There was a low correlation between D* and NF and MVD, and a low correlation was observed between T2 and R2* values and tumor volume. There was no correlation between other parameters and tumor volume, NF or MVD.

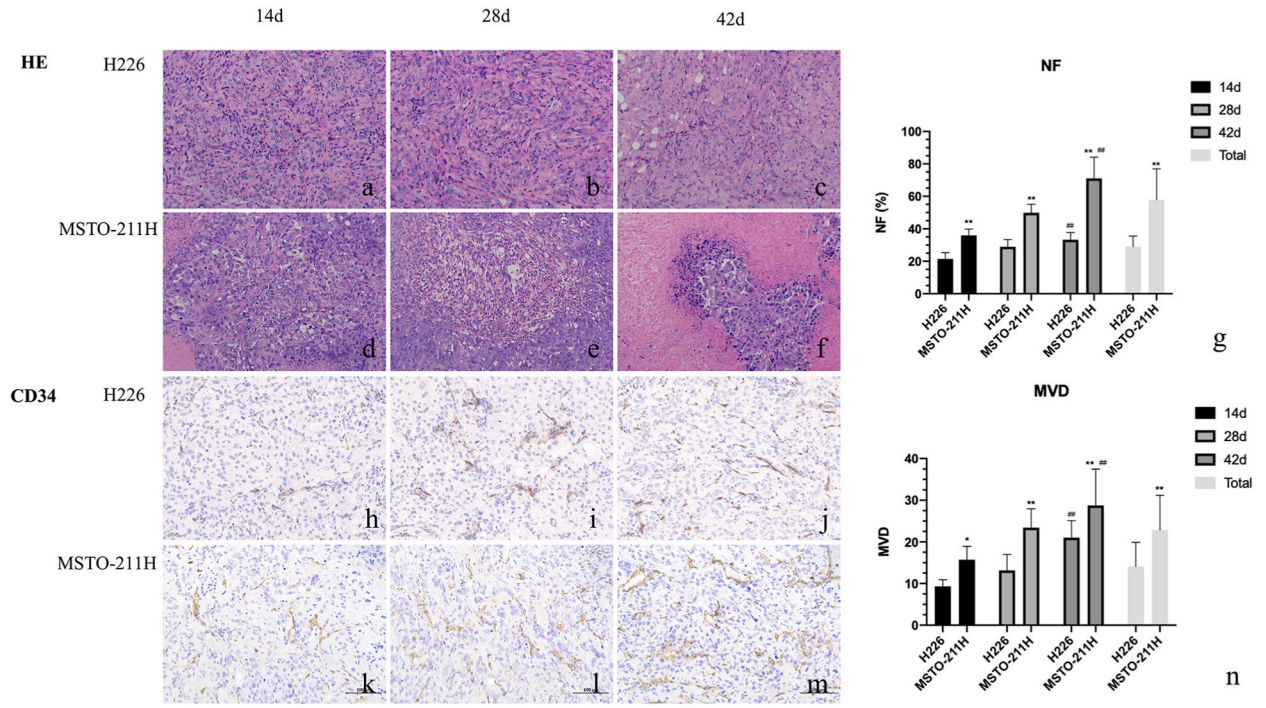

Fig. 4. Representative histopathological images of a tumor specimen with HE staining (for NF) and CD34 staining (for MVD) at day 14, day 28, and day 42 in the H226 and MSTO-211H groups. HE, first and second row (a-f, × 20); CD34 staining, third and fourth row (h-m, × 20). Necrotic tumor tissue (white arrow), microvessels in tumor tissue (black arrow). HE: hematoxylin and eosin. Data are reported as the mean ± standard deviation of the mean. #$P < 0.05$ compared with 14 days, ##$P < 0.01$ compared with 14 days, **$P < 0.01$ compared with the H226 group (Mann–Whitney U test).

Table 3
MR parameters correlate with tumor volume, NF and MVD.

	H226 (n = 21)						MSTO-211H (n = 21)					
	Tumor volume		NF		MVD		Tumor volume		NF		MVD	
Parameter	*r*	*p*	*r*	*p*	*r*	*p*	*r*	*p*	*r*	*p*	*r*	*p*
T1	0.198	0.379	0.173	0.469	0.124	0.525	0.185	0.427	0.152	0.305	0.219	0.118
T2	−0.224	0.040#	−1.630	0.139	−0.097	0.308	0.281	0.039#	0.223	0.105	0.223	0.104
R2*	0.042	0.704	0.055	0.616	0.058	0.600	−0.289	0.034#	−0.177	0.201	−0.340	0.012
T2*	−0.084	0.447	−0.089	0.423	−0.121	0.274	0.202	0.142	−0.117	0.401	−0.053	0.703
ADC	−0.53	0.000#	−0.508	0.000#	−0.44	0.000#	−0.173	0.211	−0.172	0.215	0.053	0.702
D	−0.431	0.001#	−0.456	0.000#	−0.312	0.004#	−0.055	0.715	−0.053	0.71	0.059	0.672
D*	−0.031	0.781	0.053	0.634	0.000	0.997	0.065	0.641	0.327	0.016#	0.342	0.011#
f	0.445	0.004#	0.404	0.002#	0.437	0.001#	−0.560	0.009#	−0.507	0.001#	−0.554	0.000#

Note: n, numbers of tumors; NF, necrotic fraction; MVD, micro-vessel density.

4. Discussion

Tumor histological subtypes, necrosis and angiogenesis are important prognostic factors related to the survival rate of MPM patients. Although MPM tissue samples can be obtained through pretreatment pleural biopsy, tumor heterogeneity makes it more prone to sampling errors in diffuse MPM. Multiparameter MRI may help quantitatively analyse the histological subtypes of MPM and the development of histological characteristics. This study found that T2, T2* and IVIM-DWI parameters can reflect the spatial and temporal heterogeneity of MPM and are related to important pathological indicators of MPM. Therefore, T2, T2*, and IVIM-DWI parameters can be used as potential biomarkers to assess the histopathological subtypes of MPM and show the prospect of IVIM model quantitative analysis of the histological characteristics of MPM tumors.

Liu and Carter used T2 mapping to identify benign and malignant tumors of the breast and ovary [19,20]. The results showed that the T2 value of malignant tumors was significantly lower than that of benign tumors. However, few studies have explored the value of the T2 value in identifying pathological subtypes of tumors. In this study, our results showed that the T2 and T2* values of the two types of MPM were significantly different. Previous studies have suggested that the T2WI signal intensity of cervical adenocarcinoma is

higher than that of squamous cell carcinoma, and the transverse relaxation time and T2 signal are closely related [21]. However, as the tumor progressed, the T2 and T2* values of H226 and MSTO-211H did not change significantly, and there was no good correlation with tumor NF and MVD.

IVIM-DWI using the biexponential DWI model can not only provide the pure diffusion coefficient (D) as a parameter of the pure diffusion of free water but also provide the pseudo diffusion coefficient (D*) and perfusion fraction (f) as parameters that reflect perfusion [22]. In our xenograft model, MSTO-211H had a larger tumor volume and lower ADC, D, D* and f values than H226. This may be related to the different degrees of differentiation of the two different pathological types of MPM. Studies have shown that the degree of differentiation of epithelial MPM is higher than that of biphasic MPM [23], while poorly differentiated tumors tend to have lower diffusion. In a previous clinical study, Sun analysed the differentiation and tumor staging of rectal cancer by IVIM parameters. The results showed that the ADC, D* and f values of well-differentiated rectal cancer were higher than those of poorly differentiated rectal cancer, and they had a certain correlation [22]. Current studies have shown that the higher the degree of tumor differentiation, the smaller the atypia and cell density of tumor cells, and the increase in the extracellular space, leading to accelerated water molecule diffusion [24,25]. Therefore, the higher the degree of differentiation, the greater the D. In this study, the correlation between the perfusion-related parameters D* and f and the histological subtypes of MPM showed that in well-differentiated epithelial MPM tumors, the capillary network is relatively developed, and MVD increases [26]. In poorly differentiated and more malignant biphasic MPM tumors, the tumor grows faster. Although its MVD also increases, the vascular structure is underdeveloped and obvious tissue necrosis occurs, resulting in a decrease in the whole tumor tissue perfusion of biphasic MPM.

Many studies have shown that the pathobiological features of malignant tumors are spatiotemporally heterogeneous [27]. At present, the results of routine patient screening based on a single puncture biopsy of local focus lack accuracy, which may affect the treatment decision and effect of patients. In addition, observation of tumors during treatment is an important reference value for adjusting the treatment regimen, which may require continuous tumor tissue sampling and analysis, and therefore faces important challenges. This study found that with increasing tumor growth time, the NF and MVD of epithelial and biphasic MPM gradually increased, and biphasic MPM was more obvious than epithelial MPM, and sequential multiparametric MRI can noninvasively, quantitatively and visually evaluate this change. At present, some studies have found that the more advanced the T stage is, the lower ADC values are, which is helpful to assess the preoperative staging of the tumor [28,29]. In our study, the ADC and D results of the two histological subtypes of MPM showed a similar decrease with tumor progression, but epithelial MPM was more significant. Our results also show that D* and f values have statistically significant differences between different stages, but D* and NF and MVD do not have a good correlation. In the two histological subtypes of MPM, the change in the f value was different. The f value of epithelial MPM was positively correlated with NF and MVD, while biphasic MPM was negatively correlated. This result showed that with the growth of MPM tumors, both MVD and NF continue to increase, but the necrosis of biphasic MPM is more obvious, and the f value of biphasic MPM is related to this decline.

Our study has three limitations. First, there was a lack of 3D tumour evaluation in heterogenous tumour. It is difficult to accurately locate the MRI parameters and MVD and NF obtained in tumor histopathological examination in the same section. Because the heterogeneity of MPM is very strong, the MVD and NF of some sections may not completely represent the angiogenesis and tissue necrosis of the entire tumor. Second, because commercial sarcomatoid MPM cell line was not accessible to us, although it was a small percentage of the MPM. Only epithelioid and biphasic cell lines were included in this study. Third, the animal sample size was limited, and although the orthotopic pleural cavity transplantation can better simulate true MPM, tumor growth is difficult to directly observe. For the purpose of this study, this study adopted a more stable method – subcutaneous axillary implantation.

In conclusion, our results suggest that the MRI functional parameters of the two MPM histological subtypes are different, and the IVIM parameters change with increasing tumor volume and provide clinically useful information about tumor diffusion and perfusion, which is helpful for evaluating tumor development and prognosis, to provide a certain reference for the clinical development of personalized treatment. And we expect that the study of these parameters in the MPM will introduce other variables.

Funding

This work is supported by Natural Science Foundation of China (No 81960310).

Acknowledgments

The authors would like to thank Professor Fan Li (Yunnan University) for supporting this research in experimental technology and equipment.

References

[1] M. Carbone, P.S. Adusumilli, H.R. Alexander Jr., P. Baas, F. Bardelli, A. Bononi, et al., Mesothelioma: scientific clues for prevention, diagnosis, and therapy, CA A Cancer J. Clin. 69 (5) (2019) 402–429.
[2] G. Gaudino, J. Xue, H. Yang, How asbestos and other fibers cause mesothelioma, Transl. Lung Cancer Res. 9 (Suppl 1) (2020) S39–s46.
[3] A.C. Bibby, S. Tsim, N. Kanellakis, H. Ball, D.C. Talbot, K.G. Blyth, et al., Malignant pleural mesothelioma: an update on investigation, diagnosis and treatment, Eur. Respir. Rev. : an official journal of the European Respiratory Society 25 (142) (2016) 472–486.
[4] L. Brcic, I. Kern, Clinical significance of histologic subtyping of malignant pleural mesothelioma, Transl. Lung Cancer Res. 9 (3) (2020) 924–933.
[5] C. Habougit, B. Trombert-Paviot, G. Karpathiou, F. Casteillo, S. Bayle-Bleuez, P. Fournel, et al., Histopathologic features predict survival in diffuse pleural malignant mesothelioma on pleural biopsies, Virchows Arch. : an international journal of pathology 470 (6) (2017) 639–646.

[6] F. Forest, A. Patoir, P. Dal Col, A. Sulaiman, F. Camy, D. Laville, et al., Nuclear grading, BAP1, mesothelin and PD-L1 expression in malignant pleural mesothelioma: prognostic implications, Pathology 50 (6) (2018) 635–641.
[7] L.T. Nickell Jr., J.P. Lichtenberger 3rd, L. Khorashadi, G.F. Abbott, B.W. Carter, Multimodality imaging for characterization, classification, and staging of malignant pleural mesothelioma, Radiographics : a review publication of the Radiological Society of North America, Inc. 34 (6) (2014) 1692–1706.
[8] R.R. Gill, Imaging of mesothelioma, Recent results in cancer research Fortschritte der Krebsforschung Progres dans les recherches sur le cancer 189 (2011) 27–43.
[9] A. Müller, A. Jurcoane, S. Kebir, P. Ditter, F. Schrader, U. Herrlinger, et al., Quantitative T1-mapping detects cloudy-enhancing tumor compartments predicting outcome of patients with glioblastoma, Cancer Med. 6 (1) (2017) 89–99.
[10] C.H. Lee, Quantitative T2-mapping using MRI for detection of prostate malignancy: a systematic review of the literature, Acta Radiol. 60 (9) (2019) 1181–1189.
[11] J. Liang, Q. Cheng, J. Huang, M. Ma, D. Zhang, X. Lei, et al., Monitoring tumour microenvironment changes during anti-angiogenesis therapy using functional MRI, Angiogenesis 22 (3) (2019) 457–470.
[12] Kim Chu Hyun, Lee Ji Hyun, Lee Ji Won, et al., Introducing a new biomarker named r2*-BOLD-MRI parameter to assess treatment response in osteosarcoma, J MAGN RESON IMAGING 56 (2) (2022) 538–546.
[13] Lefebvre Thierry, Hébert Mélanie, Bilodeau Laurent, et al., Intravoxel incoherent motion diffusion-weighted MRI for the characterization of inflammation in chronic liver disease, Eur. Radiol. 31 (3) (2021-03-01) 1347–1358.
[14] Y. Zhou, J. Liu, C. Liu, J. Jia, N. Li, L. Xie, et al., Intravoxel incoherent motion diffusion weighted MRI of cervical cancer - correlated with tumor differentiation and perfusion, Magn. Reson. Imag. 34 (8) (2016) 1050–1056.
[15] J.M. Winfield, M.R. Orton, D.J. Collins, T.E. Ind, A. Attygalle, S. Hazell, et al., Separation of type and grade in cervical tumours using non-mono-exponential models of diffusion-weighted MRI, Eur. Radiol. 27 (2) (2017) 627–636.
[16] L. Dai, X. Cui, X. Zhang, et al., SARI inhibits angiogenesis and tumour growth of human colon cancer through directly targeting ceruloplasmin, Nat. Commun. 7 (2016 Jun 29), 11996.
[17] S.H. Yang, J. Lin, F. Lu, Z.H. Han, C.X. Fu, P. Lv, et al., Evaluation of antiangiogenic and antiproliferative effects of sorafenib by sequential histology and intravoxel incoherent motion diffusion-weighted imaging in an orthotopic hepatocellular carcinoma xenograft model, J. Magn. Reson. Imag. : JMRI 45 (1) (2017) 270–280.
[18] W. Geng, K.T. Ng, C.K. Sun, W.L. Yau, X.B. Liu, Q. Cheng, et al., The role of proline rich tyrosine kinase 2 (Pyk2) on cisplatin resistance in hepatocellular carcinoma, PLoS One 6 (11) (2011), e27362.
[19] L. Liu, B. Yin, K. Shek, D. Geng, Y. Lu, J. Wen, et al., Role of quantitative analysis of T2 relaxation time in differentiating benign from malignant breast lesions, J. Int. Med. Res. 46 (5) (2018) 1928–1935.
[20] J.S. Carter, J.S. Koopmeiners, J.E. Kuehn-Hajder, G.J. Metzger, N. Lakkadi, L.S. Downs Jr., et al., Quantitative multiparametric MRI of ovarian cancer, J. Magn. Reson. Imag. : JMRI. 38 (6) (2013) 1501–1509.
[21] J.J. Chung, M.J. Kim, N.H. Cho, S. Park, J.T. Lee, H.S. Yoo, T2-weighted fast spin-echo MR findings of adenocarcinoma of the uterine cervix: comparison with squamous cell carcinoma, Yonsei Med. J. 40 (3) (1999) 226–231.
[22] H. Sun, Y. Xu, A. Song, K. Shi, W. Wang, Intravoxel incoherent motion MRI of rectal cancer: correlation of diffusion and perfusion characteristics with prognostic tumor markers, AJR American journal of roentgenology 210 (4) (2018) W139–w147.
[23] W.T. Vigneswaran, D.Y. Kircheva, V. Ananthanarayanan, S. Watson, Q. Arif, A.D. Celauro, et al., Amount of epithelioid differentiation is a predictor of survival in malignant pleural mesothelioma, Ann. Thorac. Surg. 103 (3) (2017) 962–966.
[24] S. Liu, W. Guan, H. Wang, L. Pan, Z. Zhou, H. Yu, et al., Apparent diffusion coefficient value of gastric cancer by diffusion-weighted imaging: correlations with the histological differentiation and Lauren classification, Eur. J. Radiol. 83 (12) (2014) 2122–2128.
[25] Y. Wang, G. Bai, L. Guo, W. Chen, Associations between apparent diffusion coefficient value with pathological type, histologic grade, and presence of lymph node metastases of esophageal carcinoma, Technol. Cancer Res. Treat. 18 (2019), 1533033819892254.
[26] H. Sun, Y. Xu, Q. Yang, W. Wang, Assessment of tumor grade and angiogenesis in colorectal cancer: whole-volume perfusion CT, Acad. Radiol. 21 (6) (2014) 750–757.
[27] Vitale Ilio, Shema Efrat, Loi Sherene, et al., Intratumoral heterogeneity in cancer progression and response to immunotherapy, Nat. Med. 27 (2) (2021) 212–224.
[28] W. Ao, X. Bao, G. Mao, G. Yang, J. Wang, J. Hu, Value of apparent diffusion coefficient for assessing preoperative T staging of low rectal cancer and whether this is correlated with ki-67 expression, Canadian Association of Radiologists journal = Journal l'Association canadienne des radiologistes 71 (1) (2020) 5–11.
[29] Y. Wang, D. Hu, H. Yu, Y. Shen, H. Tang, I.R. Kamel, et al., Comparison of the diagnostic value of monoexponential, biexponential, and stretched exponential diffusion-weighted MRI in differentiating tumor stage and histological grade of bladder cancer, Acad. Radiol. 26 (2) (2019) 239–246.